Infrared Detection and Characterization of Near Earth Objects

S.D. Price and M.P. Egan, Phillips Laboratory
E.F Tedesco, Mission Research Corp
T.L Murdock, General Research Corp

Infrared detection from space offers an invaluable adjunct to the ground based visible searches for the discovery and characterization of Near Earth Objects (NEOs). An infrared NEO survey compensates for the bias of visible searches to preferentially discover high albedo objects. Additionally, visual to infrared spectral signatures of NEOs are markedly different from those of the large majority of stars. This provides the basis for a bulk filter that significantly reduces the onboard signal processing required for target acquisition and track. Infrared observations reduce the uncertainty in estimating the size, and subsequently the mass, of an NEO. A geometric albedo must be assumed in order to calculate a diameter from the single band visual photometry obtained during discovery or follow-up astrometry. The estimated size is thus quite uncertain owing to the factor of 20 range in NEO geometric albedos. The modeling assumptions needed to convert an infrared observation into a diameter are more tightly constrained. An infrared observation combined with visual photometry provides the requisite information to accurately determine both the albedo and size. Since the estimate of the NEO mass depends on volume, the determinations of NEO mass from infrared derived diameters are about an order of magnitude more certain than estimates from visual photometry.

Introduction

Passive thermal emission from objects located in the inner solar system peaks in the mid-infrared (defined to be between 5 and 35 μm). This is the natural consequence of the object being in thermal equilibrium with the incident sunlight. Objects of low reflectivity, or geometric albedo, which makes them difficult to detect in the visible, absorb most of the incident sunlight. The resulting characteristic temperature and the high infrared emissivity of an NEO produces a spectral energy distribution that peaks in the mid-infrared. The three idealized models commonly used to describe the thermal emission from an airless body are discussed below. Each of these models produces the subtle effect that the emission is either independent of phase or the phase function falls off much less steeply than the visual. This means that detecting NEOs at large phase angles in the infrared has inherent advantages over visual surveys.

The apparent magnitude of an NEO is a function of the brightness of the sun, its heliocentric distance, the Earth - NEO distance, the size of the object and its reflectance properties through the albedo and phase. Orbital parameters provide accurate distances and the phase curve can be measured or reasonably assumed. That leaves the geometric albedo coupled with the projected area as the remaining unknowns. The geometric albedo and the size of the object can be accurately uncoupled using visual and infrared observations.

NEO brightness parameters

Near Earth Asteroids (NEAs) and comets have a wide range of physical characteristics, the most important of which (for the present discussion) are the reflectivity and thermal properties. We provide detailed background to support our choice of parameters in estimating the detection thresholds.

Albedo

Veeder and Tedesco (1992) have determined geometric albedos for small (diameter less than 40 km) main belt asteroids from radiometric observations. Based on this albedo distribution and the assumption that the NEAs originate in the main asteroid belt, we infer that the distribution of NEA geometric albedos has a broad peak between 0.04 and 0.2

with a long tail to the high reflectivity and some objects with an albedo as low as 0.02.

Wetherill (1988) calculated that enough asteroidal fragments from collisions in the asteroid belt interior to 2.6 AU "... are perturbed into Earth crossing orbits as a consequence of the 3:1 Jovian commensurability resonance at 2.5 AU and the ν_6 secular resonance in the innermost asteroid belt" to account for the currently estimated number of NEAs. Roughly 20-25% of the NEAs come from the inner asteroid belt near 2 AU with the remainder from the center of the belt. Tedesco and Gradie (1987) point out that NEAs also could originate near the 5:2 commensurability resonance further out at 2.8 AU. Indeed, Shoemaker et al. (1990) identified 7 of the 90 or so Earth crossing objects with Jovian commensurabilities, one at 4:1 (near the ν_6 resonance at 2 AU) 3 each at the 3:1 and 5:2 commensurabilities. Wetherill (1988) also raised the possibility that a significant minority of NEOs could be devolatilized (short period) comets.

Tedesco and Gradie (1987) corrected the visual bias for NEAs with C and S class taxons and concluded that the resulting numerical ratio was more nearly what is found in the asteroid belt near 3:1 and 5:2 commensurabilities than at the inner boundary at the 4:1 commensurability which is dominated by the high albedo E class (Gradie & Tedesco, 1982). Luu and Jewett (1989) modeled the discovery bias of NEA's using Monte Carlo techniques and found that the factor of 5 to 6 bias against discovering low albedo objects was large enough to account for the observed overabundance of bright albedo asteroids. They concluded that the C class asteroids with a mean geometric albedo of ~0.05 should be about as populous among the NEAs as the more reflective S class (mean geometric albedo of 0.2). However, Wetherill (1988) predicts an enhancement of high albedo ($p > 0.3$) E class NEAs originating at the 2 AU resonance. On the other hand, devolatilized comets among NEOs have low albedos ($p \sim 0.05$) and augment the dark population. Following what is universally assumed in the literature, we adopt the mean albedos for the C and S classes to do comparisons.

The energy balance giving rise to the infrared flux requires an estimate of the bolometric Bond albedo. The Bond albedo, A, is the product of the phase integral, q, and the visual geometric albedo, p_v, ($A = qp_v$). q is obtained by integrating over the IAU adopted visual phase function and is given by the simple expression $q = 0.29 + 0.684*G$ (Bowell, et al., 1989). Values of G range from 0 to 0.5 but, in the absence of a measured value, 0.15 is used. Thus, q ranges from .3 to .6 with 0.39 being the default value. More specifically, low albedo asteroids ($p_v \sim 0.05$, C class for example) have a mean value of G of about 0.12, moderate albedo asteroids ($p_v \sim 0.2$, S class for example) have a mean of about 0.25 and high albedo asteroids ($p_v \sim 0.45$, the E class dominant at 2 AU for example) have $\langle G \rangle \sim 0.4$. This corresponds to mean Bond albedos of 0.02, 0.09 and 0.25. In lieu of any information on the matter, the bolometric Bond albedo is assumed to be equal to the Bond albedo herein defined.

Apparent visual magnitude and energy distribution

Jewett and Luu (1989) provide a formula for the apparent visual magnitude of an asteroid:

$$m_v = m_v(sun) - 2.5 \log\left(\frac{p[D/2]^2 f}{2.24x10^{16} R^2 \Delta^2}\right) \qquad (1)$$

where $m_V(sun) = -26.74$ is the apparent solar visual magnitude, p is the geometric albedo, D is the asteroid diameter and f is the simpler version of the Lumme-Bowell-Harris phase function (Bowell et al., 1989):

$$f = 0.85e^{-3.33\,(\tan\frac{\alpha}{2})^{0.63}} + .15e^{-1.87(\tan\frac{\alpha}{2})^{1.22}} \qquad (2)$$

Bowell et al. (1989) found that this phase function is valid to at least 120°.

The visual flux is obtained from the zero point flux of 3.72×10^{-12} W cm^{-2} μm^{-1}. The solar spectrum is approximated by a 5800 K blackbody.

$$H(\lambda) = \frac{BB(\lambda, 5800K)}{BB(0.55\mu m, 5800K)} * 3.72x10^{-12} 10^{-0.4m_v} \qquad (3)$$

Infrared Spectrum

A number of thermal models have been developed to account for the infrared radiometry. The models assume that the object is spherical and, if the body rotates at all, the object's equator is in the Sun-Earth-asteroid plane (unless the pole of rotation is known). The characteristic temperature of the emission is determined by the energy balance that

requires the absorbed energy to be equal to that radiated. There are three idealized models that are used to account for the thermal emission of an airless body in space:

1) The "standard" thermal model (Lebofsky and Spencer, 1989) is widely adopted, at least for main belt asteroids. This model assumes that the surface is in instantaneous equilibrium with the solar insolation. The model applies to the situation where the surface temperature equilibrates to changes in a time much shorter than the rotation period. Thus, the object may not be rotating, is rotating very slowly or has a surface of low thermal conductivity. The temperature distribution varies as $T_{SS} \cos^{1/4} \theta$, where T_{SS} is the subsolar temperature and θ is the angle between the subsolar point and the point in question as measured from the center of the body (the temperature is zero for $\theta \geq \pi/2$)

2) The isothermal constant latitude model has been found to be more representative of a few Earth crossing asteroids. (Lebofsky et al.; 1978, 1979). In this model, the surface is assumed either to have high thermal inertia and/or the object is rotating rapidly. The result is a temperature that is constant along a given latitude. The temperature profile is maximum, with T_M, in the equatorial plane and decreases with latitude as $T_M \cos^{1/4}\phi$.

3) A highly conductive body such that the entire surface is at a single temperature. This applies to no known asteroids but is often used to approximate the infrared emission from man made objects orbiting the Earth. This model underestimates the infrared flux from NEO's.

Each model has a characteristic temperature which is given by:

$$T = \left[\frac{(1-A)W}{g\epsilon\sigma R^2}\right]^{1/4} \tag{4}$$

where:

$T = T_{SS}$, the subsolar point temperature for the standard model

$T = T_M$, the maximum (equatorial) temperature for the isothermal latitude model

$T = T_C$, the constant temperature model

A is the Bond albedo (0.019 for C types, 0.09 for S types and 0.25 for highly reflective asteroids)

W/R^2 is the solar flux at the distance of the asteroid (R); W is the solar constant (.1373 W cm^{-2})

σ is the Stefan-Boltzmann constant (5.6698×10^{-12} $Wcm^{-2}K^{-4}$)

g is a geometric parameter which

$= \eta$ (0.756) the beaming factor in the standard model

$= \pi$ for the isothermal latitude model

$= 4$ for the constant temperature model

ϵ = the infrared emissivity (0.9)

The geometry for the standard model requires g be equal to one. However, the radiation from craters is preferentially scattered in the sunward direction (Spencer, 1990) and while the model assumes it is too cold to do so, emission from the dark side of the asteroid contributes to the infrared flux. These effects are accounted for by a beaming factor η which modifies the surface temperatures by $1/\eta^{1/4}$ and an empirical phase function of ~0.01 mag/deg. The infrared emission from an asteroid of diameter, D, heliocentric distance, R, and distance from the Earth, Δ, is given by:

$$H(\lambda,D,\Delta) = \frac{\pi D^2}{4*2.24x10^{16}\,\Delta^2}\epsilon\overline{BB(\lambda)}$$

$$\overline{BB(\lambda)} = \int_0^{\pi/2} BB(\lambda, T_{SS}\cos^{1/4}\theta)\, 2\sin\theta\cos\theta\, d\theta \quad \textit{standard model} \tag{5}$$

$$= \int_0^{\pi/2} BB(\lambda, T_M\cos^{1/4}\phi)\, 2\cos\phi\, d\phi \quad \textit{isothermal constant latitude model}$$

$$= BB(\lambda, T_c) \quad \textit{isothermal model}$$

To a good approximation, the infrared magnitude is given by:

$$m_{ir} \approx -2.5 \log H(\lambda,\Delta,R) - 30.25 - 9.5 \log \lambda \tag{6}$$

The isothermal constant latitude model is phase independent as is the isothermal case. Significantly, the infrared phase function falls off less steeply with phase angle than the visual function given in Equation (2).

Influence of asteroid parameters on flux

It is obvious from Equation (1) that the visual flux is directly proportional to albedo. All other parameters being equal, a C class asteroid is about 4 times (1.5 mag.) fainter than an S class. There is a second order effect in that C class asteroids have neutral optical colors, that is, the reflectivity is independent of wavelength, while S class asteroids have reddish colors. The long recognized consequence is that, if C and S class asteroids are equally numerous, any magnitude limited visual survey of NEOs will be strongly biased against detecting the low reflectivity objects.

Because the characteristic temperature varies as the one-fourth power of the absorptive, emissive and geometric properties of the object in Equation (4), these factors influence the temperature weakly. There is only a 6% difference in the characteristic temperature in a given model between the darkest (C's) and most reflective (E's) classes of asteroids. There is only a 6% difference in T between the isothermal model and the isothermal latitude model arising from the respective values of the geometric parameter, g. The sub-solar temperature for the standard model is some 40-45% higher than the other models. The characteristic model temperature has a somewhat stronger dependence on heliocentric distance, $T \propto R^{-1/2}$.

The infrared flux is given by the nonlinear blackbody function of temperature and wavelength. The flux is very sensitive to temperature on the Wien side of the blackbody peak. Such is the situation in the mid-infrared for objects in the main belt (Apollo and Amors at aphelia). Here, there are significant differences between the fluxes predicted by the standard and isothermal latitude models. Marsden (private communication) proposes that a good NEO survey strategy would be to observe the NEOs at aphelia, when they are moving slowly with small phase angles. Figure 1 shows the spectral energy distributions for C type asteroids 1 km in diameter at opposition 2 and 2.9 AU from the Sun, the region encompassing the Jovian commensurabilities from which the NEOs originate. The upper curve to each energy distribution is from the standard model while the lower is from the isothermal constant latitude model. Also, shown are the 10th and 20th magnitude curves. The infrared flux from the standard thermal model is about the same as the visual flux with the consequent $m_v - m_{ir} > 10$ to 11. The visual flux would be 4 times (1.5 mag.) greater for an S class asteroid but the decrease in infrared flux would be barely distinguishable in the Figure.

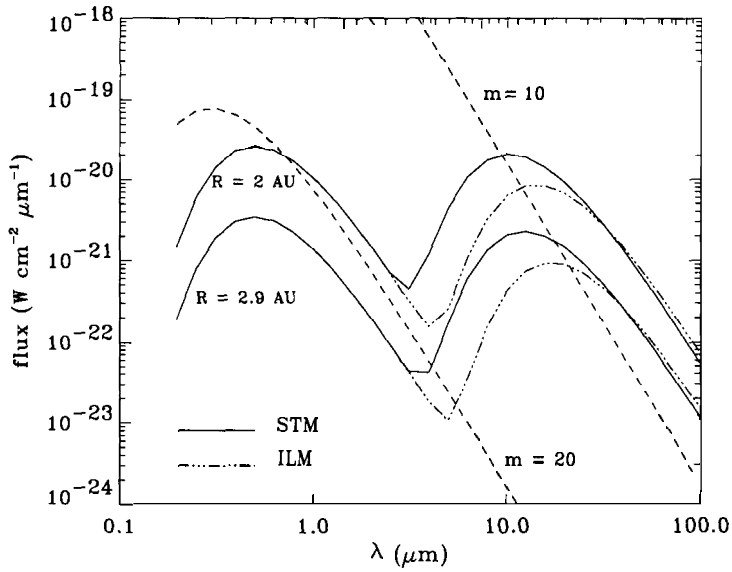

Figure 1 Spectra measured at Earth from 1 km diameter C class asteroids 2 AU and 2.9 AU from the sun. STM refers to the "standard" thermal model of Lebofsky and Spencer (1989). ILM refers to the isothermal constant latitude model. 10th and 20th magnitude curves are plotted for comparison.

If the temperature is high enough and/or the wavelength long enough, the blackbody function approximates the

Rayleigh-Jeans energy distribution which is proportional to temperature. There is not much difference in the fluxes predicted by the different thermal models. This is the situation in the mid-infrared for NEOs interior to the Earth's orbit. Interior to the Earth's orbit the phase function becomes significant. To demonstrate this we examine the scenario posed by Hills and Leonard (1995). Figure 2 shows the apparent brightness of a 100 m object, 10 days from impact with the Earth and traveling at a relative speed of 10 km/sec. Since the stated objective of Hills and Leonard was to detect "most" objects we use a C class geometric albedo of 0.05 for the visual fluxes and the E class bolometric bond albedo of 0.25 for the thermal model. Figure 2 does, indeed, confirm the Hills and Leonard observation that the infrared is better at detecting NEOs at large phase angles (small solar elongations). The fluxes predicted using the standard thermal model and the isothermal constant latitude model are roughly a factor of two higher than that from the isothermal (conductive) model used by Hills and Leonard.

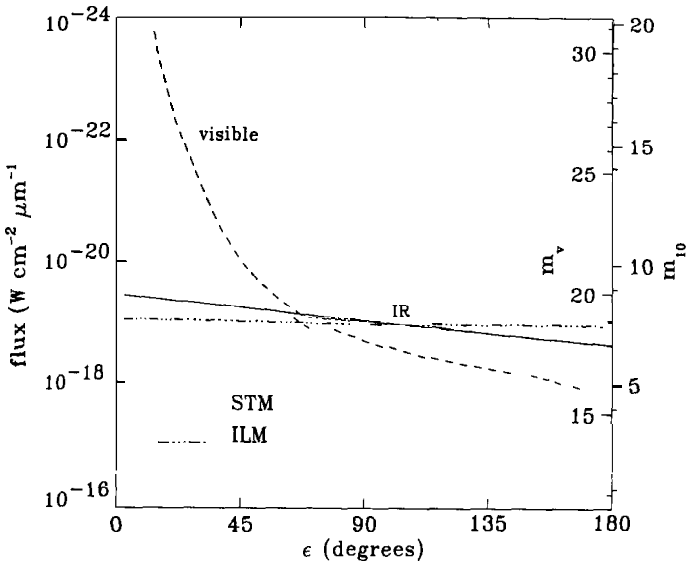

Figure 2 Brightness of a 0.1 km diameter asteroid as a function of solar elongation angle. The visible (0.55 μm) curve assumes C class albedo, while the IR (10.6 μm) curves assume E class. The right hand y-axis is scaled for visual and IR apparent magnitude.

The main points in this section are:

- The majority of Near Earth Objects likely originate in the main asteroid belt. Their taxonomies, reflective and absorptive properties should reflect that of their origins. Therefore, a large number, if not the majority, of objects will be of low reflectivity.
- The large proportion of highly reflective asteroids among the known NEOs is due to a discovery bias that visual surveys have against dark objects. This bias has been estimated at 5:1. One must use a geometric albedo representative of the low reflectivity objects in estimating the visual survey performance required to detect the majority of objects down to a given size.
- The visual phase function is steep for phase angles greater than 90°, making visual searches difficult interior to the Earth's orbit.
- In the infrared, the assumed or adopted parameters have a weak influence on the mid-infrared flux. An infrared survey will be only slightly biased against the minority of objects whose observed mid-infrared flux is consistent more with the isothermal constant latitude model than the standard model. An infrared survey is invaluable in compensating for the low reflectivity bias of ground based visual searches.
- The infrared phase function is nonexistent or weak compared to that in the visual. An infrared survey would be advantageous in discovering objects at large phase angles.

The Infrared Advantage

Background

Infrared observations from the ground must be made through the atmosphere. Atmospheric absorption limits the observations to "window" regions. Emission from both the atmosphere and telescope create a photon noise which is the ultimate limit to the performance of an infrared detection system. Variations in the atmospheric emission and absorption can produce a much larger "sky noise." These sources of noise are reduced by using small instantaneous fields of view and, in some cases, beam switching. Beam switching consists of alternatively viewing two adjacent areas of sky, one containing the field of interest, the other a blank field. Differencing the two fields cancels out the variations in atmospheric emission which is correlated. The closer the two fields the higher the correlation. Small instantaneous fields of view and the current limits to focal plane device format (256x256 pixels) make ground based, large area infrared searches for NEOs impossible.

A space-based system does away with atmospheric problems. Furthermore, the vacuum of space permits the optical system and focal planes to be cooled to a temperature where self emission is no longer a limiting factor. Price (1988) provides a historical review of surveys including the space-based efforts up to and including the Infrared Astronomical Satellite (IRAS). The first space based mid-infrared detections of asteroids were made during the AFGL probe rocket survey; LeVan and Price(1984) published information on the subset of asteroids for which far infrared observations were obtained. By far the largest mid-infrared asteroid survey is "The IRAS Minor Planet Survey' (Tedesco, 1992) which contains measurements on more than 2,000 asteroids. While the IRAS survey strategy provided for revisiting an area of sky within hours after it was surveyed and, therefore, could detect object motion, it did not have the continuous revisits necessary for identification and track. Thus, IRAS requires that the asteroid have a known, reliable orbit in order to identify it by means of a position match. The IRAS Minor Planet Survey has about a 10-15% efficiency in detecting the higher numbered asteroids (Tedesco, et al., 1992). Thus, an additional 300 or so detections lurk in the IRAS data based on the increase in the numbered minor planets since mid-1991 when the known minor planet input catalog was frozen for the IRAS Minor Planet Survey.

Currently, there are three major infrared experiments either manifested for flight or being constructed. The Infrared Space Observatory (ISO) is an observatory class experiment with small (3 arcmin) fields of view designed to obtain spectroscopy, photometry and small area imagery. The optical system has a 0.6 m primary aperture and super-critical helium for an 18-month lifetime. The Wide-field Infrared Experiment (WIRE) is a NASA sponsored "MIDEX" program designed to obtain very sensitive imagery over a few tens of square degrees in two mid-infrared spectral bands during a 4-month mission. WIRE has a 0.3 m optical system with two128x128 arrays with diffraction sized pixels. The SPIRIT III instrument on the Midcourse Space Experiment (MSX) has a one-third meter unobscured optical system cooled with solid hydrogen (Mill et al., 1994). MSX has several experiments planned to survey several hundred square degrees with the line scanned arrays.

Feasibility

The Space Infrared Telescope Facility (SIRTF) is a meter class instrument which is currently supporting technology development in all areas of space based infrared technology (Werner and Bothwell, 1993). Edison (Thronson, private communication) is a design concept for a 1.7 meter instrument which makes full use of passive, or radiative, cooling for an extended lifetime.

Thus, given the technology both demonstrated and in hand, most of the hardware capability for a space based infrared survey for Near Earth Objects is extant. In the near future, more sensitive focal planes will be developed as will sophisticated hybrid (active plus passive) cooling for an extended lifetime. We estimate the following reasonable physical characteristics of such a system.

Sensitivity and spatial resolution drive us to a large optical system. A one meter telescope is well within current technology. Furthermore, we select an unobscured aperture not only for the clear collecting area but for the superior off-axis rejection when operating at relatively small angles to a bright source, the Sun or Moon for example. We propose two mid-infrared spectral bands, 6-14μm and 17-25μm. A third visual CCD provides visual - infrared color discrimination between stars and NEOs. The optics should be diffraction limited at 12 μm with the pixels sized to 2.44*(12 μm)/1 m, i.e., 6".

Focal plane manufacturers list current device capability as < 150 noise electrons at a 10 Hz sampling rate. The noise electrons per second is given by:

$$N_e = \frac{e_n}{t_s} \quad \frac{\textit{noise electrons/sample}}{\textit{seconds/sample}} \tag{7}$$

To get the equivalent photon flux, this expression has to be divided by the quantum yield, the efficiency of the detector in converting photons to electrons. This quantity is usually taken as a constant, 0.9. The efficiency is actually a function of wavelength, $\eta(\lambda)$ [note the η parameter is redefined] and is the factor that causes the relative response curve to depart from the ideal λ/λ_p variation. The number of photons per second equivalent to the noise electrons in Equation (7) is

$$N_{ph} = \frac{e_n}{t_s \eta(\lambda)} \quad \textit{photons/sec.} \tag{8}$$

The equivalent total power in the noise is $N_{ph}h\nu$ and

$$NEP = N_{ph}h\nu = \frac{e_n}{t_s \eta(\lambda)} \frac{hc}{\lambda} \quad \textit{watts} \tag{9}$$

Normalizing to λ_p:

$$NEP = \frac{e_n}{t_s \eta(\lambda_p)} \frac{hc}{\lambda_p} \left[\frac{\eta(\lambda_p)}{\eta(\lambda)} \frac{\lambda_p}{\lambda}\right] \tag{10}$$

The inverse of the quantity in brackets is the relative response of the detector, designated R_D. Note that since R_D is a function of wavelength the NEP is an inverse function of wavelength. A peak wavelength of 23 μm is representative for Si:As BIB detectors. The peak wavelength corresponds to the energy between the valence and conduction bands in this material. Longer wavelength response arises from impurity energy levels lying above the valence band.

Assuming the rather modest device improvement in the near future will produce readout noise of 100 noise electrons for a 10 msec sample interval, the NEP becomes:

$$\begin{aligned} NEP &= \frac{100}{0.01 \cdot 0.9} \frac{2x10^{-19}}{23} R_D^{-1} \quad \textit{watt} \\ &= 10^{-16} R_D^{-1} \quad \textit{watts} \end{aligned} \tag{11}$$

The noise equivalent flux density (NEFD) at wavelength, λ, is the NEP given in Equation (11) divided by the effective collecting area:

$$NEFD = \frac{NEP}{A_c \tau_M \tau_f \tau_e} \quad W\ cm^{-2} \tag{12}$$

where:

$A_c = 7854$ cm² and is the collecting area of an unobscured 1 meter optical system.

τ_M = the total reflectivity of the mirrors in the optical system

τ_f = the transmission of the filter and dichroic.

τ_e = the energy from the point response function encompassed by a pixel.

The spectral NEFD is obtained by dividing Equation (12) by the response weighted spectral bandwidth

$$NEFD = \frac{4}{\pi \cdot 10^4} \frac{10^{-16}}{\int_{-\lambda_1}^{\lambda_2} \tau_M \tau_f \tau_\theta R_D \, d\lambda} = \frac{1.3x10^{-20}}{\int_{-\lambda_1}^{\lambda_2} \tau_M \tau_f \tau_\theta R_D \, d\lambda} \; W \; cm^{-2} \; \mu m^{-1} \qquad (13)$$

For nominal values for the τ's, the response weighted bandwidth (the integral in the denominator) and equal intensity effective wavelength are about 2.2 μm and 10.5 μm, respectively, for the 6-14 μm spectral band and about 5 μm and 21 μm, respectively, for the 17-25 μm band. The single sample sensitivities are, therefore, $6x10^{-21}$ and $2x10^{-21}$ W cm^{-2} μm^{-1} at 10.5 and 21 μm, respectively.

The focal planes baselined for the sensor are line scanned arrays with eight columns in the scan direction, four on either side of a half pixel offset. On board signal processing will use a matched filter tuned to the nominal point response to eliminate low frequency background (*e.g.* zodiacal emission) and increase the signal to noise. With a 4 samples per pixel scan rate the "visibility" of the tuned filter and the time delay and integrate of the 4 in line pixels increases the point source detection sensitivity by a factor of 4.4. We adopt a signal to noise threshold of 6 for detection, a common value used for infrared systems. The detection threshold for our system is, therefore, $8x10^{-21}$ and $3x10^{-21}$ W cm^{-2} μm^{-1} at 10.5 and 21 μm, respectively. (These fluxes correspond to the respective infrared magnitudes of ~10.5 and ~7.)

We see, from Figure 1, that the system can easily detect the 1 km diameter asteroid at 2 AU. At 2.9 AU the system would be limited to detecting objects with diameters greater than 2.5 km. The system would have no problem detecting the 100 m object in the scenario given in Figure 2.

Summary

The known Near Earth Objects are predominately highly reflective. There is a discovery bias inherent in visual surveys against dark objects. For a given size, the dark objects are at least a factor of four fainter in the visual than those with high albedo. Various analyses argue that the population of dark objects among the NEOs should be at least as great as the highly reflective objects. The difference in the infrared fluxes from high and low albedo objects is relatively small, with slightly more flux coming from the dark object. A 1 m class space based infrared NEO surveillance capability is within the current state-of-the-art technology. Such a system would be an invaluable adjunct to the ground based visual survey to compensate for the bias against the smaller, dark objects and to monitor the region at relatively small solar elongations.

References

Bowell, E., Hapke, B, Domingue, D., Lumme, K., Peltoniemi, J., and Harris, A. W., "Application of Photometric Models to Asteroids", in *ASTEROIDS II*, Binzel, R.P., Gehrels, T., and Matthews, M.S. (Eds), 524 (1989).

Gradie, J.C. and Tedesco, E.F., "Compositional Structure of the Asteroid Belt", *Science*, **216**, 1405 (1982).

Hills, J.G., and Leonard, J.T., "Earth Crossing Asteroids: the Last Days Before Impact", *Astron. J.*, **109**, 401 (1995).

Lebofsky, L. A., Veeder, G. J., Lebofsky, M. J., and Matson, D. L., "Visual and radiometric photometry of 1580 Betulia", *Icarus*, **35**, 336 (1978).

Lebofsky, L. A., Lebofsky, M.J., and Riecke, G. H., "Radiometry and surface properties of Apollo, Amor and Aten objects", *Astron. J.*, **84**, 885 (1979).

Lebofsky, L.A. and Spencer, J.A., "Radiometry And Thermal Modeling Of Asteroids", in *ASTEROIDS II*, Binzel, R.P., Gehrels, T., and Matthews, M.S. (Eds), 128 (1989).

LeVan, P.D, and Price, S. D., "85-μm Fluxes from Asteroids: 2 Pallas, 7 Iris, 15 Eunomia and 45 Eugenia," *Icarus*, **57**, 35-41 (1984)

Luu, J., and Jewett, D., "On The Relative Numbers Of C Types And S Types Among Near-Earth Asteroids", *Astron. J.*, **98**, 1905 (1989).

Mill, J. D., O'Neil, R. R., Price, S, Romick, G.J., Uy, O. M., Gaposchkin, E.M, Light, G. C., Moore, Jr., W.W., Murdock, T.L, and Stair, A. T., "The Midcourse Space Experiment: An Introduction to the Spacecraft Instrument and Scientific Objectives", *J. Spacecraft and Rockets*, **31**, 900 (1994).

Shoemaker, E. M., Wolfe, R.F., and Shoemaker, C. S., "Asteroid and comet flux in the neighborhood of Earth", in *Global*

catastrophes in Earth history; An interdisciplinary conference on impacts, volcanism and mass mortality, Sharpton, V.l., and Ward, P.D. (eds), Geological Soc. Amer. Special paper 247, 155 (1990).
Spencer, J.R., "A Rough-Surface Thermophysical Model for Airless Planets", *Icarus*, **78**, 27, (1990).
Price, S. D., "The Infrared Sky: A Survey Of Surveys", *Publ. Astron. Soc. Pac.*, **100**, 171 (1988).
Tedesco, E.F., Tholen, D.J., and Zellner, B. "The eight-color asteroid survey: Standard stars", *Astron. J.*, **87**, 1585–1592. (1982).
Tedesco, E. G., and Gradie, J, "Discovery Of M Class Objects Among The Near-Earth Asteroid Population", *Astron. J.*, **93**, 738 (1987)
Tedesco, E. F., Williams, J. G., Matson, D. L., Veeder, G. J., Gradie, J. C., and Lebofsky, L. A., "A three-parameter asteroid taxonomy", *Astron. J.*, **97**, 580–606 (1989).
Tedesco, E.F., *The IRAS Minor Planet Survey*, Phillips Laboratory, Hanscom Air Force Base, MA, PL-TR-92-2049 (1992).
Tedesco, E.F., Fowler, J.W., and Chester, T.J., "Summary", Ch. 8 of *The IRAS Minor Planet Survey*, PL-TR-92-2049 (1992).
Tedesco, E.F., "Asteroid albedos and diameters", In *Asteroids, Comets, Meteors, 1993*, A. Milani *et al.*, eds., pp. 55–74, Kluwer Academic Publishers, Dordrecht/Boston/London (1994).
Veeder, G. J., and Tedesco, E.F., "Results From The IRAS Minor Planet Survey", Ch. 7 of *The IRAS Minor Planet Survey*, PL-TR-92-2049 (1992).
Werner, M.W., and Bothwell, M., "The SIRTF Mission", *Adv. In Space Res.*, (1993)
Wetherill, G.W., "Where Do Apollo Objects Come From?" *Icarus*, **76**, 1 (1988).